

Linköping University Post Print

Spectroscopic ellipsometry study on the dielectric function of bulk Ti_2AlN , Ti_2AlC , Nb_2AlC , $(\text{Ti}_{0.5}\text{Nb}_{0.5})_2\text{AlC}$, and Ti_3GeC_2 MAX-phases

Arturo Mendoza-Galvan, M Rybka, Kenneth Järrendahl, Hans Arwin, Martin Magnuson, Lars Hultman and Michel Barsoum

N.B.: When citing this work, cite the original article.

Original Publication:

Arturo Mendoza-Galvan, M Rybka, Kenneth Järrendahl, Hans Arwin, Martin Magnuson, Lars Hultman and Michel Barsoum, Spectroscopic ellipsometry study on the dielectric function of bulk Ti_2AlN , Ti_2AlC , Nb_2AlC , $(\text{Ti}_{0.5}\text{Nb}_{0.5})_2\text{AlC}$, and Ti_3GeC_2 MAX-phases, 2011, Journal of Applied Physics, (109), 013530.

<http://dx.doi.org/10.1063/1.3525648>

Copyright: American Institute of Physics

<http://www.aip.org/>

Postprint available at: Linköping University Electronic Press

<http://urn.kb.se/resolve?urn=urn:nbn:se:liu:diva-65629>

Spectroscopic ellipsometry study on the dielectric function of bulk Ti_2AlN , Ti_2AlC , Nb_2AlC , $(\text{Ti}_{0.5}, \text{Nb}_{0.5})_2\text{AlC}$, and Ti_3GeC_2 MAX-phases

A. Mendoza-Galván,^{1,2,a)} M. Rybka,² K. Järrendahl,² H. Arwin,² M. Magnuson,² L. Hultman,² and M. W. Barsoum³

¹*Cinvestav-Querétaro, Libramiento Norponiente 2000, 76230 Querétaro, Mexico*

²*Department of Physics, Chemistry and Biology, Linköping University, SE-581 83 Linköping, Sweden*

³*Department of Materials Science and Engineering, Drexel University, Philadelphia, Pennsylvania 19104, USA*

(Received 21 August 2010; accepted 9 November 2010; published online 14 January 2011)

The averaged complex dielectric function $\varepsilon = (2\varepsilon_{\perp} + \varepsilon_{\parallel})/3$ of polycrystalline Ti_2AlN , Ti_2AlC , Nb_2AlC , $(\text{Ti}_{0.5}, \text{Nb}_{0.5})_2\text{AlC}$, and Ti_3GeC_2 was determined by spectroscopic ellipsometry covering the mid infrared to the ultraviolet spectral range. The dielectric functions ε_{\perp} and ε_{\parallel} correspond to the perpendicular and parallel dielectric tensor components relative to the crystallographic c -axis of these hexagonal compounds. The optical response is represented by a dispersion model with Drude–Lorentz and critical point contributions. In the low energy range the electrical resistivity is obtained from the Drude term and ranges from $0.48 \mu\Omega \text{ m}$ for Ti_3GeC_2 to $1.59 \mu\Omega \text{ m}$ for $(\text{Ti}_{0.5}, \text{Nb}_{0.5})_2\text{AlC}$. Furthermore, several compositional dependent interband electronic transitions can be identified. For the most important ones, $\text{Im}(\varepsilon)$ shows maxima at: 0.78, 1.23, 2.04, 2.48, and 3.78 eV for Ti_2AlN ; 0.38, 1.8, 2.6, and 3.64 eV for Ti_2AlC ; 0.3, 0.92, and 2.8 eV in Nb_2AlC ; 0.45, 0.98, and 2.58 eV in $(\text{Ti}_{0.5}, \text{Nb}_{0.5})_2\text{AlC}$; and 0.8, 1.85, 2.25, and 3.02 eV in Ti_3GeC_2 . © 2011 American Institute of Physics. [doi:10.1063/1.3525648]

I. INTRODUCTION

The MAX-phases are compounds with the chemical formula $\text{M}_{n+1}\text{AX}_n$, where M is a transition metal, A is an element from column 13 to 16 in the periodic table, and X represents C or N ($n=1, 2$, or 3). These materials are potentially technologically important as they show unique refractory and other physical properties that combine some of the best of metals and ceramics. In the scientific literature there are many reports on the processing of bulk MAX-phases as well as on their physical properties such as electrical, thermal, and elastic.^{1–6} Also, the electronic properties of these materials have been studied both theoretically and experimentally.^{4–9} For MAX-phases in thin film form, the processing and physical properties have been recently reviewed.¹⁰ Because the MAX-phases crystallize in a hexagonal structure the anisotropy of its conductivity is of great interest but it has been difficult to experimentally resolve this issue.^{11,12}

From a fundamental point of view the band structure of these materials is of interest and it is important to determine optical reference data. Optical information is contained in the complex dielectric function $\varepsilon = \varepsilon_1 + i\varepsilon_2$, where the imaginary part is the macroscopic quantity most directly related to electronic interband transitions (IBTs). The complex dielectric function has been theoretically calculated for a few MAX-phase materials like Ti_3SiC_2 , Ti_4AlN_3 ,¹³ and M_2SnC .¹⁴ In another report the pseudodielectric function of bulk and thin films of Ti_2AlN and Ti_2AlC was determined by spectroscopic ellipsometry (SE) in the ultraviolet-visible spectral range.¹² In short, not much work has been carried out on the

optical properties of these materials which has motivated us to perform the current investigation to contribute to a better understanding of electronic properties of MAX-phase materials.

SE—a nondestructive technique used for the optical characterization of surfaces and thin films—has been applied on an ample variety of materials and has been established in different fields.^{15,16} Ellipsometry is suitable for sampling areas of millimeter in size extracting information on composition and structural properties of surfaces and layers. The aim of this work is to apply SE to investigate the complex dielectric function in a wide spectral range covering the mid infrared, IR, to ultraviolet, UV, range of Ti_2AlN , Ti_2AlC , Ti_3GeC_2 , Nb_2AlC , and $(\text{Ti}_{0.5}, \text{Nb}_{0.5})_2\text{AlC}$ —the latter henceforth referred to as TiNbAlC . These measurements and subsequent analysis will result in determination of the optical properties and the electrical dc resistivity as well as the identification of several electronic IBTs, which depend on composition.

II. EXPERIMENTAL

A. Synthesis and sample preparation

The following compositions were examined: Ti_2AlN , Ti_2AlC , Ti_3GeC_2 , Nb_2AlC , and TiNbAlC . The processing details can be found elsewhere. In brief, both the Ti_2AlN and Ti_2AlC samples were fabricated by pressureless sintering of prereacted powders (3-ONE-2, Vorhees, NJ) at 1500°C for 1 h under Ar.⁶ Bulk polycrystalline Ti_3GeC_2 samples were prepared by hot pressing the appropriate stoichiometric composition of Ti, graphite, and Ge powders at 1500°C for 6 h under an applied pressure of 45 MPa. The samples were then annealed at 1500°C for 48 h in an Ar atmosphere.¹⁷ Stoi-

^{a)}Electronic mail: amendoza@qro.cinvestav.mx.

chiometric mixtures of graphite, Al_4C_3 , Ti and/or Nb were hot isostatically pressed at 1600 °C for 8 h to make the Nb_2AlC or the TiNbAlC samples.¹⁸ All samples were fully dense and predominantly single phase. Prior to the SE measurements, the samples were mounted in epoxy and their surfaces were polished using a Buehler's polishing equipment operating at 260–310 rpm. The first two polishing steps were performed using abrasive paper and a diamond solution with decreasing grit size from 3 to 1 μm . The last polishing step was performed with 0.25 μm diamond slurry. Finally, the samples were rinsed with distilled water and dried with nitrogen gas. Using this procedure the samples exhibited a metalliclike mirror finish.

B. SE measurements

In order to cover a wide spectral range, the SE measurements were performed using two ellipsometric systems from J. A. Woollam Co., Inc. For the IR, measurements—in the 480–7000 cm^{-1} (0.059–0.8 eV) range—a rotating compensator IR spectroscopic ellipsometer (IRSE) was used with a resolution of 4 cm^{-1} . The second system was a variable angle spectroscopic ellipsometer (VASE) of rotating analyzer type covering the near IR to UV spectral range. By using two different optical fibers in the latter system two spectral ranges were covered: one in the 230–1700 nm (5.39–0.73 eV) range, the other in the 300–2200 nm (4.13–0.56 eV) range. However, issues like different light beam spot sizes (that measure different areas) of the IRSE and VASE systems and sample alignment precluded the matching of the SE data in the common spectral range of the two instruments, viz., the 0.73–0.8 eV or 0.56–0.8 eV range depending on the fiber used in the VASE system. Nevertheless, it was possible to obtain a set of measurements with a good match of data for all samples but covering different spectral ranges. Therefore, as will be noticed in the figures for Ti_2AlN , Ti_2AlC , and Nb_2AlC the data are analyzed in the 0.06 to 5.4 eV range whereas those of TiNbAlC and Ti_3GeC_2 in the 0.06 to 4.13 eV range. All SE measurements were obtained at three angles, 60°, 65°, and 70°.

SE measures the change in the polarization state that a polarized light beam at oblique incidence experiences due to interaction with a sample. The optical response of nonmagnetic materials having hexagonal symmetry is described with a diagonal dielectric tensor $\text{diag}(\varepsilon_{\perp}, \varepsilon_{\perp}, \varepsilon_{\parallel})$ in the principal-axis frame, i.e., components perpendicular ε_{\perp} and parallel ε_{\parallel} to the c -axis. For single crystal arbitrarily oriented with respect to the laboratory coordinate frame, the Euler angles φ , ψ , and θ can be used to rotate among two frames by using $\mathbf{A}\text{diag}(\varepsilon_{\perp}, \varepsilon_{\perp}, \varepsilon_{\parallel})\mathbf{A}^{-1}$, where \mathbf{A} is the orthogonal rotation matrix. In that case, generalized ellipsometry should be used.¹⁵

However, for polycrystalline hexagonal samples the optical response observable by macroscopic techniques correspond to some angular average of $\mathbf{A}\text{diag}(\varepsilon_{\perp}, \varepsilon_{\perp}, \varepsilon_{\parallel})\mathbf{A}^{-1}$. For example, optical investigations carried out by SE in the IR and visible-UV ranges of polycrystalline hexagonal BN films, with the c -axis tilted an angle Θ respect to the normal surface^{19,20} have proved the applicability of this procedure

after averaging over the Euler angle φ . Completely averaged c -axis orientations of the grains within the sample give an isotropic behavior of hexagonal materials with a dielectric function,^{19,20}

$$\varepsilon = \frac{2\varepsilon_{\perp} + \varepsilon_{\parallel}}{3}, \quad (1)$$

and the formalism of standard ellipsometry is applicable. In such situations, the change in light polarization is described by the complex-valued ratio ρ between the reflection coefficients for light polarized parallel (r_p) and perpendicular (r_s) to the plane of incidence,¹⁵ viz.,

$$\rho = \frac{r_p}{r_s} = \tan \Psi \exp(i\Delta), \quad (2)$$

where ρ is expressed in terms of the two ellipsometric angles Ψ and Δ . These angles depend on the microstructure and complex dielectric functions of constituents of the sample. Thus, the construction of an optical model for the reflection coefficients r_p and r_s allows the determination of parameters like film thicknesses, complex dielectric functions, volume fractions, etc., of a multilayer model representing the sample. Those parameters are obtained in a fitting procedure that minimizes the mean square error (MSE) between the model and experimental data,

$$\text{MSE} = \frac{1}{2N - M} \sum_{i=1}^N \left[\left(\frac{\Psi_i^{\text{mod}} - \Psi_i^{\text{exp}}}{\sigma_{\Psi_i}^{\text{exp}}} \right)^2 + \left(\frac{\Delta_i^{\text{mod}} - \Delta_i^{\text{exp}}}{\sigma_{\Delta_i}^{\text{exp}}} \right)^2 \right], \quad (3)$$

where N is the number of Ψ – Δ measured pairs, M the total number of fit parameters, and σ^{exp} are the standard deviations of the measurements. The superscripts mod and exp indicate model-calculated and experimental data, respectively. The nonlinear regression algorithm also provides 90% confidence limits of the fitted parameters. In this work the data fitting were performed with the WVASE32 software (J. A. Woollam Co., Inc.).

III. RESULTS AND DISCUSSION

A. Modeling and data analysis

Figure 1 shows the ellipsometric spectra Ψ and Δ of the MAX-phases measured in the mid-IR to UV spectral range at the three angles of incidence. The experimental data are shown with discontinuous lines; the best model fits by the continuous lines obtained with the model described below. In Fig. 1, several features attributable to electronic IBTs are observed, which are more specifically characterized by maxima, minima, and other changes in the slopes of the complex dielectric functions. However, as ε is unknown for these materials the use of some analytical expression has to be considered. All the MAX-phases studied herein are excellent electrical conductors, which can be included in the model dielectric function, assuming,

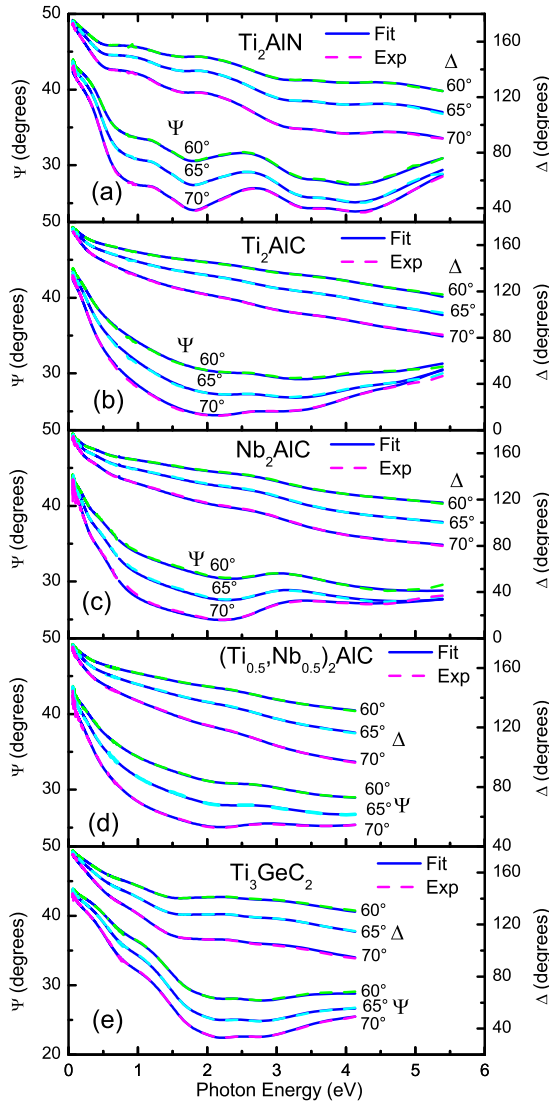


FIG. 1. (Color online) Experimental and best fit ellipsometric spectra at three angles of incidence (60° , 65° , and 70°) for (a) Ti_2AlN , (b) Ti_2AlC , (c) Nb_2AlC , (d) TiNbAlC , and (e) Ti_3GeC_2 . The changes in slope of Ψ and Δ spectra below 1 eV reveal the onset of IBTs at those photon energies.

$$\varepsilon(E) = \varepsilon_\infty + \varepsilon_{IB}(E) - \frac{\left(\frac{\hbar}{\varepsilon_0 \rho_{dc}}\right) \left(\frac{\hbar}{\tau_0}\right)}{E(E + i\hbar/\tau_0)}, \quad (4)$$

where E is the photon energy, ε_∞ is the high-energy dielectric constant, $\varepsilon_{IB}(E)$ represents interband electronic transitions and the third term, the so-called Drude expression, corresponds to the free carrier contributions, where ε_0 is the permittivity of the free space, \hbar is the reduced Planck constant, τ_0 is the collision time of the free carriers, and ρ_{dc} is the dc electrical resistivity. The second term in Eq. (4), ε_{IB} , is the sum of the Lorentz harmonic oscillator and critical points line shapes, namely,

$$\varepsilon_{IB}(E) = \sum_{j=1}^s \frac{A_j B_j E_{0j}}{E_{0j}^2 - E^2 - iB_j E} + L_{cp}(E), \quad (5)$$

where E_{0j} is the central energy, A_j the amplitude, B_j the broadening of the j th oscillator, and the number of terms, s , depends on composition. The line shape of the critical points

L_{cp} in turn depends on the dimensionality and type (for three-dimensional M_0 -minimum, M_1 and M_2 -saddle, M_3 -maximum).¹⁵

The characteristic results of a bulk sample shown in Fig. 1, $\Psi < 45^\circ$ and $\Delta < 180^\circ$, do not necessarily imply a perfectly flat air-sample interface because some surface roughness can be expected due to the polishing procedure. Therefore, the use of a transition layer between the air and sample is required. Herein, the transition layer is represented by the Bruggeman effective medium approximation¹⁵ as a 50%–50% mixture of voids and the MAX-phase material. Thus, the ellipsometric data were analyzed using an air/intermix/MAX-phase model where the intermix layer thickness, as well as, the various parameters listed in Eqs. (4) and (5) are fitted.

For the fitting procedure, the number of oscillators and the initial guesses of the parameters in Eq. (5) have to be assigned with caution. As a first step, the number of oscillators and their parameters can be estimated by analyzing the pseudodielectric function obtained by direct inversion of Eq. (2) assuming a film-free air/substrate system,¹⁵ viz.,

$$\langle \varepsilon \rangle = \sin^2 \phi \left[1 + \tan^2 \phi \left(\frac{1 - \rho}{1 + \rho} \right)^2 \right], \quad (6)$$

where ϕ is the angle of incidence. Figure 2 shows the $\langle \varepsilon \rangle$ data of the MAX-phases studied for the three angles of incidence measured. The fact that the three measured angles coincide (Fig. 2) indirectly confirms the isotropic polycrystalline nature of the hexagonal materials assumed in Eq. (1). In the lower photon energies, the effect of free carriers is clearly seen by the negative values of $\langle \varepsilon_1 \rangle$ and the large values of $\langle \varepsilon_2 \rangle$. Also, changes in the slope of $\langle \varepsilon_1 \rangle$ and $\langle \varepsilon_2 \rangle$ reveal several IBTs, which are more prominent at photon energies higher than ~ 1 eV.

The second step of the analysis systematically varies the model parameters to minimize the error [viz., Eq. (3)]. Nevertheless, depending on the number of terms considered in the summation of Eq. (5), some differences between the experimental and fitted spectra are noticeable. A better resolution of the small features can be obtained from derivative spectra of Ψ and Δ data. With this procedure it is possible to determine whether or not the number of oscillator considered is appropriate. As an example, Figs. 3(a) and 3(b) show the excellent agreement between experimental and model of the first derivative spectra of Ψ and Δ , respectively, obtained for the Ti_2AlN sample using seven terms for the IBTs. Additionally, second (or higher order) derivatives can be considered as shown in Figs. 3(c) and 3(d). Applying this procedure the fitting parameters were obtained with a MSE of the order of unity. Table I shows the intermix layer thickness, the high-energy dielectric constant ε_∞ , and Drude parameters used in Eq. (4). For comparison, some literature dc resistivity values are also included.

The thickness of the intermix layer ranges between 6.2 nm for TiNbAlC to 37.9 nm for Ti_3GeC_2 (Table I). The reliability of the larger values and the applicability of the Bruggeman expression can be questioned. However, SE studies of silicon-on-sapphire samples have shown that the

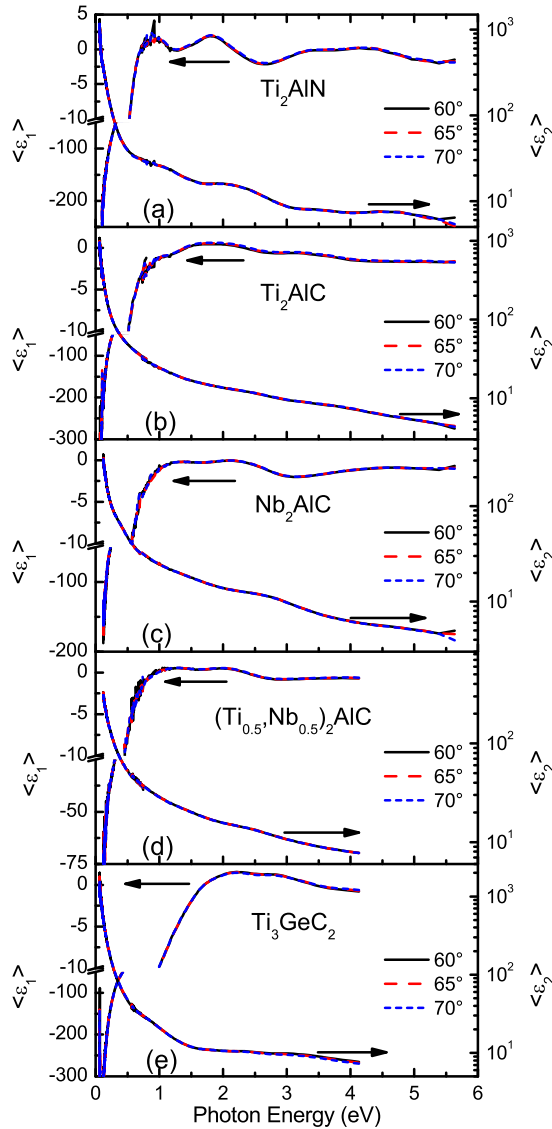


FIG. 2. (Color online) Pseudodielectric function of MAX-phases measured at the three angles of incidence for (a) Ti_2AlN , (b) Ti_2AlC , (c) Nb_2AlC , (d) TiNbAlC , and (e) Ti_3GeC_2 . Notice the break of scale for $\langle \epsilon_1 \rangle$ and the logarithmic scale for $\langle \epsilon_2 \rangle$.

effective medium approximation can be applied to describe their optical properties for surface layers as thick as 30 nm.^{21,22} In those papers, a graded structure consisting of mixtures of amorphous and crystalline Si plus voids was considered. Herein, the loss of crystallinity at the surface was not considered because of the lack of optical data for amorphous MAX-phases or other additional information. Hence for simplicity a 50%–50% mixture was chosen over a graded structure with a depth-dependent void fraction since the latter approach increases the number of fitting parameters. Furthermore, as discussed below, the analysis performed on the derivatives of the ellipsometric spectra lends further support for the absolute values of the complex dielectric functions obtained.

B. Electrical resistivity

As noted above, the MAX-phases studied in this work are good electrical conductors, with metalliclike conduction

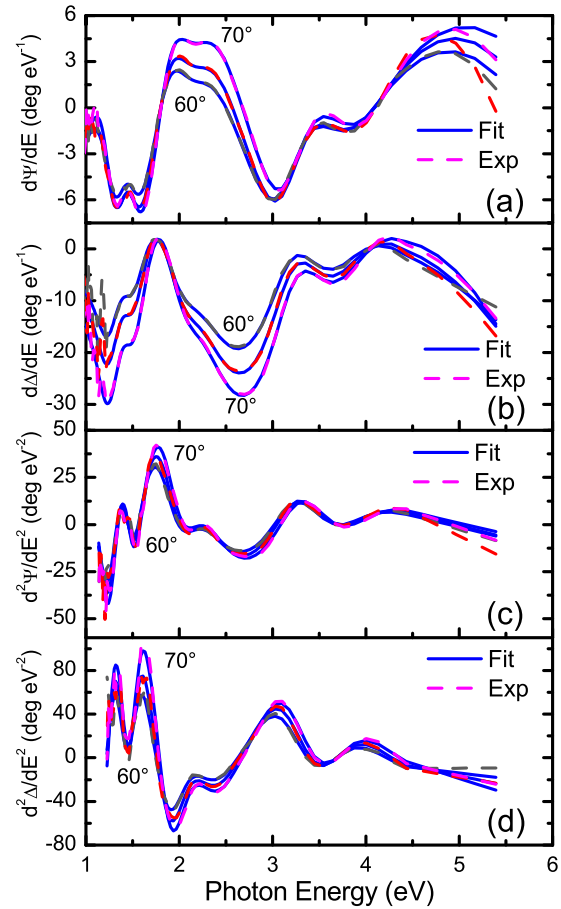


FIG. 3. (Color online) Experimental and best fits of the first (a) and (b) and second (c) and (d) derivative ellipsometric spectra of Ti_2AlN for photon energies higher than 1.0 eV. Notice the small features in both derivative spectra of Ψ and Δ at about 1.5 eV.

dominated by the d -states of the transition metal. Carrier concentrations are of the order of 10^{27} m^{-3} with equal contributions of electrons and holes, i.e., they are compensated conductors.^{2,4,6} As seen in Table I, the resistivity values obtained in this work, through the Drude term, are within a factor of 2 to 3.5 of those reported for bulk materials measured using a four-probe technique. When the two sets of

TABLE I. Values of the intermix layer thickness d , high-energy dielectric constant ϵ_∞ , and parameters in the Drude term in Eq. (4). For comparison, literature resistivity values from dc measurements are included.

Sample	d (nm)	ϵ_∞	$\hbar\tau_0^{-1}$ (eV)	ρ_{dc} ($\mu\Omega \text{ m}$)		
				This work	dc measurements	EELS
Ti_2AlN	25.8	-2.87	0.33	0.84	0.34 ^a	0.66 ^b
Ti_2AlC	28.3	-0.48	0.18	0.84	0.37 ^a	0.81 ^b
Nb_2AlC	8.2	-1.21	0.15	1.17	0.40 ^c	...
$(\text{Ti}_{0.5}, \text{Nb}_{0.5})_2\text{AlC}$	6.2	-0.27	0.33	1.59	0.78 ^d	...
Ti_3GeC_2	37.9	-1.97	0.38	0.48	0.25 ^e	...

^aReference 6.

^bReference 12.

^cReference 2.

^dReference 23.

^eReference 4.

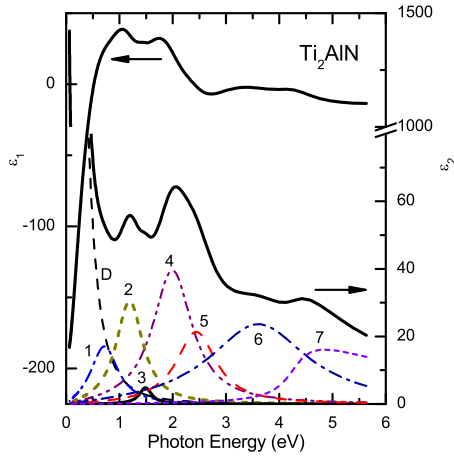


FIG. 4. (Color online) Averaged complex dielectric function $\varepsilon = \varepsilon_1 + i\varepsilon_2$ of Ti_2AlN . Notice the break of scale for ε_2 . At the bottom are shown the contributions of the intraband (D-Drude term) and IBTs to ε_2 , labeled as D and numbered 1–7, respectively. Labels for the IBTs are with reference to Table II: Lorentz type 1 to 6 and transition 7 is a critical point of M_1 type.

results are plotted against each other (not shown) a least-squares correlation coefficient, R^2 , of 0.87 is obtained. Furthermore, the least-squares curve almost goes through the origin as it should.

Using electron energy loss spectroscopy (EELS) data, the resistivity along the $[100]$ and $[001]$ directions has been calculated.¹² By averaging those resistivities according to, $\rho_{\text{av}}^{-1} = (2\rho_{[100]}^{-1} + \rho_{[001]}^{-1})/3$, values of 0.66 and 0.81 $\mu\Omega\text{ m}$ for Ti_2AlN and Ti_2AlC are obtained, respectively, and have been included in Table I. Clearly, the latter values are in a better agreement with our results than those from dc measurements. In thin film form, dc resistivity values of 0.39, 0.44, 0.9, and 0.50 $\mu\Omega\text{ m}$ have been reported for epitaxial Ti_2AlN ,²⁴ Ti_2AlC ,²⁵ Nb_2AlC ,²⁶ and Ti_3GeC_2 ,²⁷ respectively. The resistivities of the two latter compounds as well that reported of $\approx 1.45\ \mu\Omega\text{ m}$ for $(\text{Ti}_{0.49}\text{Nb}_{0.51})_2\text{AlC}$ thin films²⁸ are in a good agreement with our data in Table I.

In Table I the values of collision energies $\eta\tau_0^{-1}$ are below 0.4 eV indicating that the free carrier behavior is limited to low energies. It should be mentioned that a frequency-dependent collision time $\tau^{-1} = \tau_0^{-1} + \beta\omega^2$ suggestive of electron–electron scattering²⁹ was considered but the results were not as good as those with a single relaxation time. Thus, the limited range of free carrier behavior makes a precise determination of the resistivity by optical means diffi-

TABLE II. Parameters of IBTs in Eq. (5) for Ti_2AlN . The IBT type is specified as Lorentz, L, or critical point, M_1 .

Transition	E_{0j} (eV)	A_j	B_j (eV)	Type
1	0.78	16.3	0.64	L
2	1.23	29.9	0.62	L
3	1.49	4.8	0.28	L
4	2.04	39.1	0.89	L
5	2.48	21.2	0.90	L
6	3.78	23.1	2.26	L
7	4.28	8.6	0.33	M_1

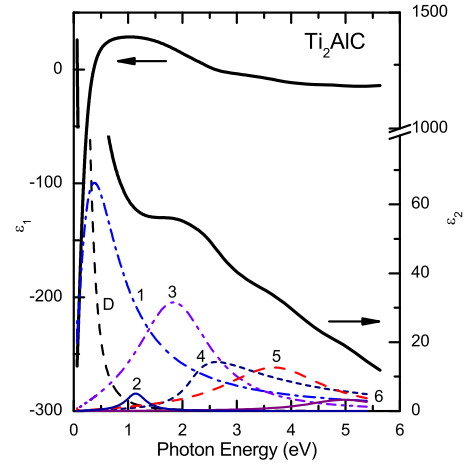


FIG. 5. (Color online) Complex dielectric function $\varepsilon = \varepsilon_1 + i\varepsilon_2$ of Ti_2AlC . Notice the break of scale for ε_2 . At the bottom are shown the contributions of the intraband (D) and IBTs. The latter correspond to M_0 (1), M_1 (4), and Lorentz (2, 3, 5, and 6) types with parameters given in Table III.

cult. This is in contradistinction to the case of TiN , where the free electrons response extends up to frequencies in the visible range.³⁰

C. Dielectric function

Figure 4 shows the obtained complex dielectric function $\varepsilon = \varepsilon_1 + i\varepsilon_2$ of Ti_2AlN . The free carrier contribution is clearly identified by the negative values of ε_1 and the large ε_2 values for photon energies below 1.0 eV. For clarity, the ε_2 axis is broken, which allows for the identification of the individual contributions of the Drude term (D) and the seven identified IBTs as shown at the bottom. The latter corresponds to six Lorentz oscillators and a critical point of type M_1 with parameters given in Table II. The smallest IBT at 1.49 eV (no. 3), difficult to be distinguished on the scale of the figure, had to be included to describe the first and second derivative features of the SE spectra at that photon energy shown in Fig. 3. According to the density of states (DOS) reported for Ti_2AlN , several maxima below and above the Fermi level, E_F , are present.^{5,7} Thus, it is possible that electronic IBTs occur from states just below E_F to bands just above it giving rise to the critical points observed in ε_2 . Because of the unavailability of data for Ti_2AlN and for comparison purposes we consider the theoretically calculated dielectric function of the Ti_4AlN_3 MAX-phase.¹³ In that work, in addition to the IBTs obtained from the band structure calculations, the authors considered a Drude term with plasma and collision

TABLE III. Parameters of IBTs in Eq. (5) for Ti_2AlC . The IBT type is specified as Lorentz, L, or critical point, M_j .

Transition	E_{0j} (eV)	A_j	B_j (eV)	Type
1	0.02	34.1	0.46	M_0
2	1.16	5.03	0.45	L
3	2.01	30.2	1.66	L
4	2.20	9.32	0.32	M_1
5	3.84	12.4	2.26	L
6	5.04	3.23	1.63	L

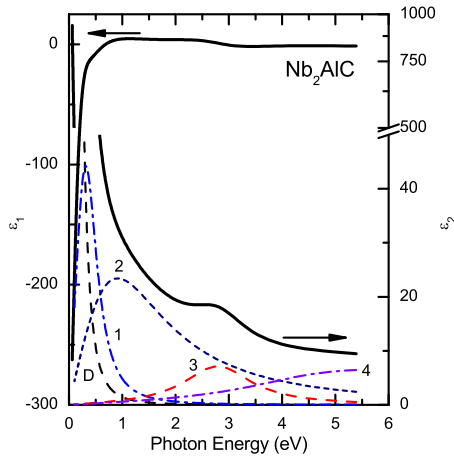


FIG. 6. (Color online) Complex dielectric function $\varepsilon = \varepsilon_1 + i\varepsilon_2$ of Nb_2AlC . Notice the break of scale for ε_2 . At the bottom are shown the contributions of the intraband (D) and four IBTs: two of Lorentz type (2 and 3) and two of M_1 critical point (1 and 4). The corresponding parameters are given in Table IV.

energies of 1.0 eV and 0.3 eV, respectively. Herein, the corresponding values are 5.38 and 0.33 eV. Nevertheless, it is noticeable that ε shows a similar dispersion in both compounds: ε_1 shows the stronger dispersion below 2 eV in Ti_4AlN_3 and Ti_2AlN below 2.5 eV (see Fig. 4). On the other hand, the pseudodielectric complex function $\langle \varepsilon \rangle$ shown in Fig. 2(a) is similar to that previously reported¹² but with higher values of $\langle \varepsilon_1 \rangle$ at lower photon energies and in $\langle \varepsilon_2 \rangle$ along the whole measured range. These differences can be attributed to differences in surface quality and/or composition.

The dielectric function for Ti_2AlC (Fig. 5) was modeled using a Drude term plus six IBTs. The contribution of each term is shown at the bottom of the figure and corresponds to four Lorentz oscillators (nos. 2, 3, 5, and 6) and two critical points: one of type M_0 (no. 1) and another of type M_1 (no. 4). The resulting parameters are listed in Table III where it can be noticed that the center energy of the M_0 transition is 0.02 eV but its maximum is at 0.38 eV, Fig. 5. The contribution of electronic IBTs at photon energies as low as 0.1 eV has been reported for TiC_x .³¹ According to band structure calculations for Ti_2AlC , the maxima in the DOS are closer to E_F than in Ti_2AlN .^{5,7} This fact could explain the origin of the strong IBT at lower energies in the former compound. For comparison, band structure calculations reported that ε_2 for Ti_2SnC show several IBT below 6 eV, with significant contributions of Drude behavior for energies below 1 eV.¹⁴ Unfortunately, a direct comparison cannot be made because, (i) the authors

TABLE IV. Parameters of IBTs in Eq. (5) for Nb_2AlC . The IBT type is specified as Lorentz, L, or critical point, M_1 .

Transition	E_{0j} (eV)	A_j	B_j (eV)	
1	0.39	107.9	0.92	M_1
2	0.41	39.2	0.55	L
3	2.89	6.99	1.57	L
4	4.15	6.83	1.72	M_1

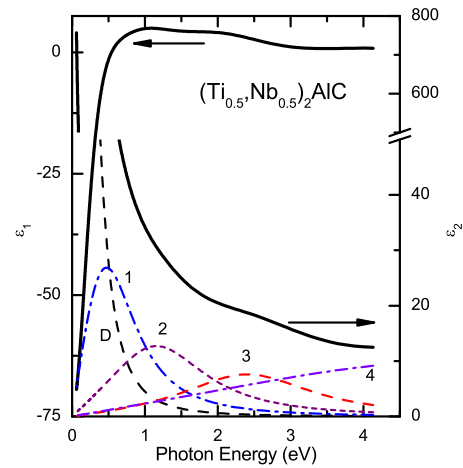


FIG. 7. (Color online) Complex dielectric function $\varepsilon = \varepsilon_1 + i\varepsilon_2$ of TiNbAlC . Notice the break of scale for ε_2 . At the bottom are shown the contributions of the intraband (D) and four (1–4) IBTs of Lorentz type with parameters given in Table V.

used atomic units in the calculations and did not specify the Drude parameters and (ii) the chemistries are different.

It is instructive at this point to compare the pseudodielectric complex function shown in Fig. 2(b) with that previously reported.¹² $\langle \varepsilon_2 \rangle$ shows similar dispersion, but our data are higher by a factor of three along the common measured range, whereas $\langle \varepsilon_1 \rangle$ shows a different dispersion. The origins of these differences are not totally clear at this time, but as noted above for Ti_2AlN , could be associated to different qualities of the sample surfaces.

In the case of Nb_2AlC (Fig. 6), the IBTs were represented by two Lorentz oscillators (nos. 1 and 3) and two critical points of type M_1 (nos. 2 and 4); the resulting parameters are listed in Table IV. In the theoretical study on the physical and chemical properties of $M_2\text{SnC}$ MAX-phases it was shown that substitution of Ti by Nb causes an overall shift in the structure in ε_2 to higher photon energy and a decrease in strength.¹⁴ In the present work, a similar result was found as can be seen by comparing Figs. 5 and 6. The values of ε_2 for Ti_2AlC are clearly higher than those for Nb_2AlC and the IBT at 2.01 eV (no. 3 in Fig. 5) in the former can be associated with that at 2.89 eV (no. 3 in Fig. 6) in the latter. This is also in agreement with the shift in the calculated DOS for these materials.^{5,7} The explanation of the IBT at lower photon energies would require a detailed analysis of the band structure of Nb_2AlC .

Figure 7 shows the complex dielectric function of TiNbAlC , the parameters of the four Lorentz oscillators, representing the IBTs of this solid solution are given in Table V.

TABLE V. Parameters of IBTs of the Lorentz type in Eq. (5) for TiNbAlC .

Transition	E_{0j} (eV)	A_j	B_j (eV)
1	0.69	22.4	1.14
2	1.42	11.5	1.76
3	2.63	7.26	2.21
4	6.59	8.85	8.65

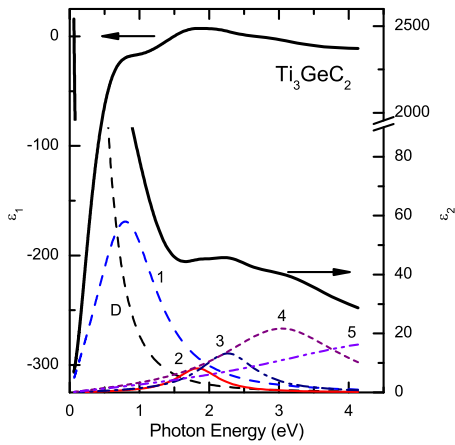


FIG. 8. (Color online) Complex dielectric function $\varepsilon = \varepsilon_1 + i\varepsilon_2$ of Ti_3GeC_2 . Notice the break of scale for ε_2 . At the bottom are shown the contributions of the intraband (D) and four (1–4) IBTs of Lorentz type with parameters given in Table VI.

Following the ideas of the previous paragraph, it would be expected that substitution of one of the Nb atoms by a Ti atom in the Nb_2AlC compound would shift the structure of ε_2 to lower photon energies. In Fig. 7 this can be seen comparing the IBT at 2.63 eV (no. 3) to that at 2.89 eV in Fig. 6 (no. 3). Furthermore, in Table I, TiNbAlC shows a collision frequency twice that of either Ti_2AlC or Nb_2AlC . This can be related to the result of the M planes are corrugated in this solid solution, which could in turn explain the stronger scattering of carriers by the M atoms in this solid solution.⁷ Consistently, as seen in Table I, the resistivity of TiNbAlC is higher than the end members Ti_2AlC and Nb_2AlC of the solid solution.

Figure 8 shows the complex dielectric function for Ti_3GeC_2 , which is represented by a Drude contribution plus five Lorentzian terms. The respective parameters are listed in Table VI. These IBTs can be related to the reported DOS for this compound,³ which showed several maxima about 1.5 eV below E_F . For comparison, we consider the theoretically calculated dielectric function of the isoelectronic Ti_3SiC_2 MAX-phase.¹³ In that work, the authors reported several IBTs at photon energies lower than 6.0 eV plus a Drude term with collision and plasma energies of 0.3 eV and 2.0 eV, respectively. The former value is similar to the 0.38 eV value obtained for Ti_3GeC_2 herein but the latter is lower than the 7.6 eV calculated with the parameters listed in Table I. Higher values of the Drude parameters increase appreciably the values of ε_2 and decrease ε_1 for photon energies below 1.5 eV. Regarding the onset of the IBTs the changing slope in

the ellipsometric data is a clear evidence of its effect at about 0.9 eV, as seen in Fig. 1(e). On the scale of Fig. 7 the IBTs look broad, but their width is comparable to those calculated for the isoelectronic compound Ti_3SiC_2 .¹³

IV. SUMMARY AND CONCLUSIONS

SE was used to measure the averaged complex dielectric function of polycrystalline bulk Ti_2AlN , Ti_2AlC , Nb_2AlC , TiNbAlC , and Ti_3GeC_2 MAX-phases. The averaged value corresponds to $(2\varepsilon_{\perp} + \varepsilon_{\parallel})/3$ of the tensor components perpendicular, ε_{\perp} , and parallel, ε_{\parallel} , to the c -axis of these hexagonal compounds. The analysis was performed by using an analytical expression that includes a free carrier contribution of the Drude type and electronic IBTs represented by Lorentz harmonic oscillators and critical point line shapes. The resistivity evaluated from the Drude term is comparable with data from previous dc measurements. It was found that the free carriers contribute to the dielectric response for photon energies lower than 1.0 eV. However, IBTs also contribute in this spectral range. For the photon energy range studied, 7, 6, 4, 4, and 5 IBTs for Ti_2AlN , Ti_2AlC , Nb_2AlC , TiNbAlC , and Ti_3GeC_2 , respectively, were identified. Where available and the IBTs transitions showed good agreement with previous band structure calculations of related MAX-phases.

ACKNOWLEDGMENTS

A.M.-G. acknowledges Conacyt-Mexico (Grant No. 80814) for the partial support to spend a sabbatical leave at Linköping University. The Knut and Alice Wallenberg Foundation is acknowledged for financial support to instrumentation. M.B. and L.H. acknowledge the Swedish Strategic Research Foundation. This work was also partially supported by a Grant from the Ceramics Division of the National Science Foundation (Grant No. DMR 0503711).

TABLE VI. Parameters of Lorentz type IBTs in Eq. (5) for Ti_3GeC_2 .

Transition	E_{0j} (eV)	A_j	B_j (eV)
1	0.96	52.9	1.14
2	1.87	8.1	0.74
3	2.32	13.1	0.98
4	3.21	21.1	2.12
5	5.24	16.4	4.76

¹M. W. Barsoum, M. Ali, and T. El-Raghy, *Metall. Mater. Trans. A* **31**, 1857 (2000).

²J. D. Hettinger, S. E. Lofland, P. Finkel, T. Meehan, J. Palma, K. Harrell, S. Gupta, A. Ganguly, T. El-Raghy, and M. W. Barsoum, *Phys. Rev. B* **72**, 115120 (2005).

³L. Chaput, G. Hug, P. Pécheur, and H. Scherrer, *Phys. Rev. B* **75**, 035107 (2007).

⁴P. Finkel, B. Seaman, K. Harrell, J. Palma, J. D. Hettinger, S. E. Lofland, A. Ganguly, M. W. Barsoum, Z. Sun, S. Li, and R. Ahuja, *Phys. Rev. B* **70**, 085104 (2004).

⁵S. E. Lofland, J. D. Hettinger, K. Harrell, P. Finkel, S. Gupta, M. W. Barsoum, and G. Hug, *Appl. Phys. Lett.* **84**, 508 (2004).

⁶T. Scabarozzi, A. Ganguly, J. D. Hettinger, S. E. Lofland, S. Amini, P. Finkel, T. El-Raghy, and M. W. Barsoum, *J. Appl. Phys.* **104**, 073713 (2008).

⁷G. Hug, M. Jaouen, and M. W. Barsoum, *Phys. Rev. B* **71**, 024105 (2005).

⁸M. Magnuson, O. Wilhelmsson, J.-P. Palmquist, U. Jansson, M. Mattesini, S. Li, R. Ahuja, and O. Eriksson, *Phys. Rev. B* **74**, 195108 (2006).

⁹M. Magnuson, M. Mattesini, S. Li, C. Höglund, M. Beckers, L. Hultman, and O. Eriksson, *Phys. Rev. B* **76**, 195127 (2007).

¹⁰P. Eklund, M. Beckers, U. Jansson, H. Höglund, and L. Hultman, *Thin Solid Films* **518**, 1851 (2010).

¹¹V. Mauchamp, G. Hug, M. Bugnet, T. Cabioch, and M. Jaouen, *Phys. Rev. B* **81**, 035109 (2010).

¹²N. Haddad, E. Garcia-Caurel, L. Hultman, M. W. Barsoum, and G. Hug, *J. Appl. Phys.* **104**, 023531 (2008).

¹³S. Li, R. Ahuja, M. W. Barsoum, P. Jena, and B. Johansson, *Appl. Phys. Lett.* **92**, 221907 (2008).

¹⁴M. B. Kanoun, S. Goumri-Said, and A. H. Reshak, *Comput. Mater. Sci.*

- 47, 491 (2009).
- ¹⁵H. G. Tompkins and E. A. Irene, *Handbook of Ellipsometry* (William Andrew, New York, 2005).
- ¹⁶*Proceedings of the Fourth International Conference on Spectroscopic Ellipsometry*, edited by H. Arwin, U. Beck, and M. Schubert (Wiley, Weinheim, 2008) [*Phys. Status Solidi A* **205**, 709 (2008)]; [*Phys. Status Solidi C* **5**, 1003 (2008)].
- ¹⁷A. Ganguly, T. Zhen, and M. W. Barsoum, *J. Alloys Compd.* **376**, 287 (2004).
- ¹⁸I. Salama, T. El-Raghy, and M. W. Barsoum, *J. Alloys Compd.* **347**, 271 (2002).
- ¹⁹M. Schubert, B. Rheinländer, E. Franke, H. Neumann, J. Hahn, M. Röder, and F. Richter, *Appl. Phys. Lett.* **70**, 1819 (1997).
- ²⁰M. Schubert, E. Franke, H. Neumann, T. E. Tiwald, D. W. Thompson, J. A. Woollam, and J. Hahn, *Thin Solid Films* **313–314**, 692 (1998).
- ²¹C. Pickering, in *Photonic Probes on Surfaces*, edited by P. Halevi (Elsevier, Amsterdam, 1995).
- ²²C. Pickering, A. M. Hodge, A. C. Daw, D. J. Robbins, P. J. Pearson, and R. Greef, *Semiconductor-on-Insulator and Thin Film Transistor Technology*, edited by A. Chiang, M. W. Geis, and L. Pfeiffer, MRS Symposia Proceedings No. 53 (Materials Research Society, Pittsburgh, 1986), p. 317.
- ²³M. W. Barsoum, I. Salama, T. El-Raghy, J. Golczewski, W. D. Porter, H. Wang, H. J. Seifert, and F. Aldinger, *Metall. Mater. Trans. A* **33**, 2775 (2002).
- ²⁴T. Joelsson, A. Horling, J. Birch, and L. Hultman, *Appl. Phys. Lett.* **86**, 111913 (2005).
- ²⁵O. Wilhelmsson, J.-P. Palmquist, T. Nyberg, and U. Jansson, *Appl. Phys. Lett.* **85**, 1066 (2004).
- ²⁶T. H. Scabarozzi, J. Roche, A. Rosenfeld, S. H. Lim, L. Salamanca-Riba, G. Yong, I. Takeuchi, M. W. Barsoum, J. D. Hettinger, and S. E. Lofland, *Thin Solid Films* **517**, 2920 (2009).
- ²⁷H. Högberg, P. Eklund, J. Emmerlich, J. Birch, and L. Hultman, *J. Mater. Res.* **20**, 779 (2005).
- ²⁸T. Scarabozzi, Ph.D. thesis, Drexel University, 2009.
- ²⁹G. R. Parkins, W. E. Lawrence, and R. W. Christy, *Phys. Rev. B* **23**, 6408 (1981).
- ³⁰P. Patsalas and S. Logothetidis, *J. Appl. Phys.* **93**, 989 (2003).
- ³¹D. W. Lynch, C. G. Olson, D. J. Peterman, and J. H. Weaver, *Phys. Rev. B* **22**, 3991 (1980).